The Astrophysical Journal, 774:9 (13pp), 2013 September 1 doi:10.1088/0004-637X/774/1/9

VISCOUS EVOLUTION AND PHOTOEVAPORATION OF CIRCUMSTELLAR DISKS DUE TO EXTERNAL FAR ULTRAVIOLET RADIATION FIELDS

Kassandra R. Anderson[1,2], Fred C. Adams[1,2], and Nuria Calvet[2]
[1] Physics Department, University of Michigan, Ann Arbor, MI 48109, USA
[2] Astronomy Department, University of Michigan, Ann Arbor, MI 48109, USA
Received 2013 May 24; accepted 2013 July 15; published 2013 August 8

ABSTRACT

This paper explores the effects of FUV radiation fields from external stars on circumstellar disk evolution. Disks residing in young clusters can be exposed to extreme levels of FUV flux from nearby OB stars, and observations show that disks in such environments are being actively photoevaporated. Typical FUV flux levels can be factors of $\sim 10^2$–10^4 higher than the interstellar value. These fields are effective in driving mass loss from circumstellar disks because they act at large radial distance from the host star, i.e., where most of the disk mass is located, and where the gravitational potential well is shallow. We combine viscous evolution (an α-disk model) with an existing FUV photoevaporation model to derive constraints on disk lifetimes, and to determine disk properties as functions of time, including mass-loss rates, disk masses, and radii. We also consider the effects of X-ray photoevaporation from the host star using an existing model, and show that for disks around solar-mass stars, externally generated FUV fields are often the dominant mechanism in depleting disk material. For sufficiently large viscosities, FUV fields can efficiently photoevaporate disks over the entire range of parameter space. Disks with viscosity parameter $\alpha = 10^{-3}$ are effectively dispersed within 1–3 Myr; for higher viscosities ($\alpha = 10^{-2}$) disks are dispersed within $\sim$0.25–0.5 Myr. Furthermore, disk radii are truncated to less than $\sim$100 AU, which can possibly affect the formation of planets. Our model predictions are consistent with the range of observed masses and radii of proplyds in the Orion Nebula Cluster.

Key words: accretion, accretion disks – planets and satellites: formation – protoplanetary disks – stars: formation – stars: pre-main sequence

Online-only material: color figures

1. INTRODUCTION

Circumstellar disks provide the material out of which planets, asteroids, comets, and other solar system objects are engendered. An understanding of the time evolution of such disks is essential to explain the origins of our own solar system, and the hundreds of additional exoplanetary systems. Observed solar systems harbor planets with a wide variety of masses, compositions, and orbital elements; models of disk formation and evolution must be able to account for this dispersion in the properties of extrasolar planets.

Observations show that circumstellar disks are dispersed relatively quickly, often within 3–5 Myr and nearly always within 10 Myr (Hernández et al. 2008). This time constraint introduces the need to incorporate efficient mass depletion into existing disk theories (in addition to viscous accretion onto the host star). One standard explanation for the short observed disk lifetimes is photoevaporation by radiation fields, either by the host star, or for disks in sufficiently populated regions, by massive OB stars residing in the surrounding cluster (see Adams 2010 and Armitage 2011 for general discussions of typical environments of young star–disk systems and descriptions of disk evolution and sources of mass loss). Regardless of the source of the radiation fields, the effects on the surface density profile can be significant, thereby influencing (and possibly hindering) subsequent planet formation.

Many young star–disk systems reside in relatively isolated areas (e.g., Taurus and Chamaeleon), with low stellar densities and few or no nearby massive stars; in these regions, radiation from external stars is not high enough to affect the disk structure, and the primary source of mass loss (due to photoevaporation) is the host star itself. However, in populated regions that contain OB stars, external fields can be important and often provide more radiation than the host stars (Armitage 2000; Fatuzzo & Adams 2008; Holden et al. 2011). Circumstellar disks can thus be roughly separated into two classes based on the environment in which they reside: those living in isolation, where the disk is affected primarily by the host star, and those living in groups where external stars can influence the disk properties. A better physical understanding of the latter case is especially important because stars often form in groups rather than in isolation (Lada & Lada 2003). An immediate example of this type of environment is the Orion Nebula Cluster (ONC), which hosts the "proplyds"—distorted disks that appear to be actively photoevaporated by the Trapezium O stars, especially θ^1 C (O'Dell et al. 1993; Henney & O'Dell 1999; Bally et al. 2000). This idea is further supported by the fact that the average disk mass in the ONC appears to be lower than in Taurus, and is an order of magnitude lower than the minimum mass solar nebula (Eisner et al. 2008); thus far, no observed disks in Orion seem to have masses greater than 0.034 $M_\odot$ (Mann & Williams 2009). Disks close to the cluster center (projected distances less than 0.3 pc from θ^1 C) are inferred to have the lowest masses (Mann & Williams 2010). The luminosity of θ^1 C is high enough so that the proplyds are exposed to FUV flux levels of $G_0 \sim 10^3$–10^4 (note that $G_0 = 1$ corresponds to the typical flux in the interstellar medium, 1.6×10^{-3} erg s^{-1} cm^{-2}; Habing 1968). In contrast, T Tauri disks in isolated regions experience FUV flux from the central star only of order $G_0 \sim 10^2$ at a distance $r = 100$ AU (Bergin et al. 2003).

Many previous studies of disk photoevaporation have focused on internally generated radiation fields, i.e., from the host

star. EUV fields from the central star were first considered by Hollenbach et al. (1994); Clarke et al. (2001) subsequently combined this EUV radiation with a standard α-disk model to explore the time evolution. This work showed that EUV fields can affect the disk structure by creating an inner "hole" at a radius of order 10 AU, but usually only on long time scales—roughly a factor of 10 longer than observed disk lifetimes of ∼3–10 Myr. This conclusion led to refinements of this initial effort (Alexander et al. 2006), as well as the consideration of other types of radiation from the host star as agents of mass loss, including FUV radiation and X-rays (Gorti & Hollenbach 2009; Gorti et al. 2009; Ercolano et al. 2009). This latter work showed that both types of radiation fields can deplete material at low to moderate radii, clear gaps in the surface density, and produce disk lifetimes that are consistent with observations. Subsequent authors have considered the relative importance of these photoevaporation agents. For example, Owen et al. (2010, 2011, 2012) showed that the effects of X-rays can prevent EUV photons from heating the disk and driving a flow, and argued that X-rays could be the most important agent in disk dispersal.

Alongside this work on radiation fields from the central star, additional studies have investigated the effects of external radiation fields (due to nearby stars) on protoplanetary disk evolution (e.g., Johnstone et al. 1998; Richling & Yorke 2000; Störzer & Hollenbach 1999; Adams et al. 2004). The last of these papers presents detailed numerical simulations—and derives analytic approximations—for the expected mass-loss rates, and shows that they can be comparable to (or even higher) than mass-loss rates due to internally generated radiation fields. Subsequent papers have coupled these photoevaporation models with viscous accretion, in order to evaluate the prospects for planet formation (Mitchell & Stewart 2010), and to compare the model predictions with the disk radii of observed proplyds in the ONC (Clarke 2007).

The main goal of this paper is to combine existing photoevaporation models with time-dependent disk models in order to derive constraints on disk masses, radii, and mass-loss rates for a wide range of parameters. Here we focus on photoevaporation from external FUV sources and use the results of a previous study (Adams et al. 2004) to determine the mass-loss rates for different external FUV fluxes G_0. A secondary goal is to combine these external FUV radiation fields with X-rays from the host star, and to determine the parameters where one source of photoevaporation is more important than the other. Finally, this work shows that disks trace out well-defined evolutionary tracks in the mass–radius plane, where these tracks depend on the external (and internal) radiation fields and the viscosity parameter α. These mass–radius planes (analogous to H-R diagrams for stellar evolution) can be useful for comparing theoretical models for disk evolution with observational data.

This paper builds upon previous work in a number of ways: most prior studies have focused on internally produced radiation fields coupled with viscous disk evolution, whereas this work develops similar models for externally illuminated disks. Although external radiation fields have been considered (Armitage 2000; Clarke 2007), the parameter space has not yet been fully explored and newly available data for disk masses in the ONC (Mann & Williams 2010) allow these models to be more rigorously tested. This work presents results from a large ensemble of disk simulations, which provide disk masses, disk radii, and mass-loss rates as functions of time; we then compare the results to current data. Note that these results will be useful for future observational comparisons. We show that relatively modest external FUV radiation fields ($G_0 = 300$) can sometimes dominate the disk evolution by greatly reducing the lifetime of the disk, as well as by truncating the outer edge. This present work also differs from previous papers in that we combine our external FUV model with an existing model for X-ray evaporation from the host star (Owen et al. 2012), and we delineate the portion of parameter space where one radiation field is more important than the other. For example, disks exposed to FUV flux levels $G_0 = 3000$ are nearly always dominated by external, rather than internal, radiation fields.

One can understand the importance of external radiation as follows: while the radiation flux from the host star is strongest in the inner disk (due to its r^{-2} dependence), the flux arising from external sources is essentially constant over the entire disk (since the distance to "nearby" stars is much larger than the dimensions of the disk itself). The effects from external fields are thus most prominent in the outer regions, where mass is less tightly bound to the host star (and where the radiation from the central star is weakest). As a result, evaporation from these two sources leads to evolution that is qualitatively different: the radiation fields from the host star tend to destroy disks from the "inside out," whereas fields from external sources work from the "outside in." Since most of the mass resides in the outer regions of the disk, external radiation fields have the potential to deplete the overall disk mass on relatively short time scales.

This paper is organized as follows. Section 2 outlines our formulation of the problem, including the basic equations and assumptions. After a brief discussion of numerical techniques, Section 3 presents the results of our simulations for various FUV fluxes, disk viscosities, and X-ray luminosities. We then compare the predictions of our model with observed disk masses and radii in the ONC, and show that the model predictions are in agreement with the observations. We conclude, in Section 4, with a summary of our results, a discussion of their implications, and some suggestions for future work.

2. DISK EVOLUTION MODEL

2.1. Viscous Evolution

In the case of purely viscous evolution, the diffusion equation for the surface density Σ has the well-known form

$$\frac{\partial \Sigma}{\partial t} = \frac{3}{r}\frac{\partial}{\partial r}\left[r^{1/2}\frac{\partial}{\partial r}\left(\nu r^{1/2}\Sigma\right)\right], \tag{1}$$

where r is the radius in cylindrical coordinates and ν is the viscosity (Pringle 1981). We follow the standard α-model (Shakura & Sunyaev 1973), where the viscosity ν is given in terms of the expression

$$\nu = \alpha\frac{a_s^2}{\Omega} = \alpha\frac{k_B T}{m_{\rm H}}\left(\frac{r^3}{GM_*}\right)^{1/2}, \tag{2}$$

where α is a dimensionless parameter that determines the magnitude of viscosity, a_s is the sound speed, Ω is the Keplerian frequency, T is the midplane temperature, M_* is the host star mass, and the fundamental constants k_B, G, and $m_{\rm H}$ have the usual meaning. In this paper, we work in terms of dimensionless variables, where the radial coordinate is scaled by 1 AU and time is scaled by 1 yr; we thus define dimensionless variables through the transformation

$$r \rightarrow \frac{r}{1\ {\rm AU}} \qquad \text{and} \qquad t \rightarrow \frac{t}{1\ {\rm yr}}. \tag{3}$$

We adopt a midplane temperature profile of the form $T = T_m r^{-1/2}$, which is consistent with irradiated accretion disks (D'Alessio et al. 1999). After making these substitutions, the diffusion equation for the surface density takes the form

$$\frac{\partial \Sigma}{\partial t} = \frac{3\beta}{r}\frac{\partial}{\partial r}\left[r^{1/2}\frac{\partial}{\partial r}(r^{3/2}\Sigma)\right]. \quad (4)$$

Notice that an effective viscosity coefficient β has been introduced, where

$$\beta \equiv 2\pi\alpha\left(\frac{k_B T_m}{m_{\rm H}}\right)\left(\frac{r_0}{GM_*}\right) \approx 6\times 10^{-3}\alpha\left(\frac{M_*}{M_\odot}\right)^{-1}\left(\frac{T_m}{100\ {\rm K}}\right), \quad (5)$$

where $r_0 = 1$ AU.

Throughout this paper, standard boundary conditions for the surface density Σ are assumed, where the torque vanishes at the inner boundary r_1 (so that $\Sigma(r_1) = 0$), and where the disk is allowed to expand freely at the outer boundary. We choose an initial surface density profile of the form

$$\Sigma(r,0) = \Sigma_0\frac{\exp\left[-r/r_d\right]}{r} \approx \frac{M_d}{2\pi r_d(1-e^{-1})}\frac{\exp\left[-r/r_d\right]}{r}, \quad (6)$$

where Σ_0 provides the normalization for the surface density, and where M_d and r_d are the initial disk mass and radius. The approximation equality becomes exact in the limit $r_1 \rightarrow 0$. For the case of purely viscous evolution, the surface density approaches this form for any choice of the initial profile; we thus adopt this form to reduce the time needed for the surface density to reach its asymptotic form.

In the presence of significant radiation fields, additional mass flows are introduced through photoevaporation, and the surface density profile decreases more rapidly with time. As a general rule, photoevaporation causes mass to become unbound near (and outside) a critical radius r_g where the sound speed a_s is comparable to the escape velocity (e.g., Hollenbach et al. 1994; Adams et al. 2004). The critical radius thus has the form

$$r_g = \frac{GM_*}{a_s^2} \approx 100\ {\rm AU}\left(\frac{M_*}{1\ M_\odot}\right)\left(\frac{T}{1000\ {\rm K}}\right)^{-1}. \quad (7)$$

The effects of radiation fields are included by introducing a sink term into Equation (4), which yields

$$\frac{\partial \Sigma}{\partial t} = \frac{3\beta}{r}\frac{\partial}{\partial r}\left[r^{1/2}\frac{\partial}{\partial r}(r^{3/2}\Sigma)\right] - \dot{\Sigma}(r), \quad (8)$$

where the radial dependence of the sink term $\dot{\Sigma}$ depends upon the type of radiation field(s) under consideration.

2.2. FUV Radiation Fields Due to External Stars

We follow Adams et al. (2004) to model FUV evaporation due to external stars, who include detailed numerical calculations and semi-analytic expressions for the total mass-loss rates as a function of the FUV flux G_0. They focus on "subcritical disks," where the disk radius r_d is smaller than the gravitational escape radius r_g (see Equation (7)). In this situation, FUV photons incident at the outer disk edge penetrate radially inward and heat columns of gas. A subsonic outflow of mass then develops at the disk edge and accelerates outward; eventually the flow crosses a sonic radius r_s (with $r_d < r_s < r_g$), where the flow becomes supersonic and mass can freely escape. Since the flow originates at large distances from the host star, it can be approximated as spherically symmetric (with a limited angular extent). See Figure 1 for a schematic illustration of this process. Additional flow occurs in the vertical direction, but the radial flow dominates the mass loss in the subcritical ($r_d < r_g$) regime (Adams et al. 2004).

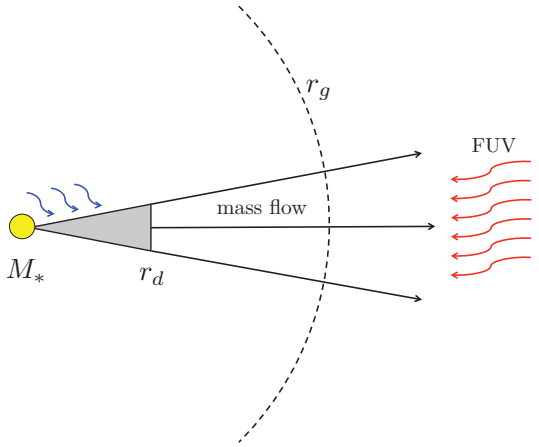

Figure 1. Illustration of a subcritical disk (with $r_d < r_g$). The disk (shown in gray) is viewed edge-on, with the gravitational radius r_g included for reference (dashed arc). Incident FUV radiation from nearby OB stars heats the gas near the disk edge and causes a nearly radial outflow of mass. Additional outflows in the vertical direction (not shown) also contribute to the total photoevaporative mass loss, but are generally small compared to the radial flow. The host star provides additional radiation (shown in blue), which includes FUV, EUV, and X-rays. This paper focuses on the effects of external FUV illumination, but also considers X-ray illumination from the host star.

(A color version of this figure is available in the online journal.)

For the case of externally illuminated disks, the critical radius r_g can be written in the form given by Equation (7). Note that the given value of $r_g \sim 100$ AU differs from the typical value quoted in the literature for internal evaporation from the host star (e.g., Clarke et al. 2001), where $r_g \sim 10$ AU is due to heating by EUV photons. This difference arises because the gas temperature in regions of EUV ionization is quite high (and nearly isothermal), where $T \sim 10^4$ K, and mass can become unbound at closer distances from the host star. In this case, however, the temperature T in Equation (7) refers to the temperature in the photodissociation region (PDR) near the outer edge, where heating is due to FUV photons and the temperature is lower ($T \sim 10^2$–10^3 K). This lower temperature is reflected in a larger gravitational radius, where $r_g \sim 100$ AU. Temperature profiles for the PDR are shown in Figure 2 of Adams et al. (2004); these temperatures are a function of external FUV field strength, as well as visual extinction A_v and gas particle density. The dependence of the FUV field strength is thus encapsulated into r_g implicitly through the temperature T.

For subcritical disks, with outer radius $r_d \lesssim r_g$, the expected mass-loss rates as a function of disk radius can be approximated by

$$\dot{M}(r) = A r_g^{3/2} r^{1/2}\exp\left[-r_g/2r\right], \quad (9)$$

where the parameter A can be expressed as

$$A = C n_d a_s \langle\mu\rangle. \quad (10)$$

The constant C is of order unity, n_d is the gas particle density at the disk edge, a_s is the sound speed at the sonic radius, and

$\langle\mu\rangle$ is the mean particle mass (see Appendix A in Adams et al. 2004 for more details). Note that $\dot{M}(r)$ represents the total mass lost due to photoevaporation up to an outer radius, and thus Equation (9) should be evaluated at $r = r_d$. We can also write $\dot{M}$ as the integral

$$\dot{M}(r) = \int_{r_1}^{r} 2\pi r' \dot{\Sigma}(r') dr' \,. \tag{11}$$

By assuming conservation of mass, we can find the mass-loss rate per unit area ($\dot{\Sigma}$) that is consistent with this total mass-loss rate, i.e.,

$$\frac{d\dot{M}}{dr} = 2\pi r \dot{\Sigma} = \frac{d}{dr}\left\{ A r_g^{3/2} r^{1/2} e^{-r_g/2r} \right\} . \tag{12}$$

Expanding the derivative and solving for $\dot{\Sigma}$, we thus obtain the expression

$$\dot{\Sigma}(r) = \frac{A}{4\pi}\left(\frac{r_g}{r}\right)^{3/2}\left[1 + \frac{r_g}{r}\right] e^{-r_g/2r} . \tag{13}$$

Equation (13) captures the basic physics of external FUV radiation and the radial dependence is dominated by the exponential term. The incident FUV flux is essentially constant (because the distance to the source is much larger than the disk radius). Gas residing in the outer regions of the disk (where the gravitational potential well is shallower) will thus experience the same FUV flux as the gas in the inner disk, and can escape more easily. Photons incident at the disk edge can penetrate inward to some extent, heat the gas, and initiate mass flow through the disk. This flow, in conjunction with mass conservation, gives rise to the radial dependence of the sink term $\dot{\Sigma}$. Since the incident radiation is exponentially attenuated moving radially inward, significant mass loss occurs primarily at larger radial distances, and the disk shrinks from the outside in.

To fully determine the mass-loss profile, the parameters (r_g, A) in Equation (13) must be specified. Recall that the dependence of the FUV field strength is implicitly included in the expression for r_g via the temperature T in Equation (7). Here we fix these parameters by fitting a function of the form given by Equation (9) to the numerical results shown in Figure 4 of Adams et al. (2004), where the mass-loss rates $\dot{M}$ are plotted as a function of outer disk radius and FUV radiation field. The results of these (non-linear) curve fits yield an escape radius $r_g = 357$ AU for a radiation field strength $G_0 = 300$, $r_g = 157$ AU for $G_0 = 3000$, and $r_g = 90$ AU for $G_0 = 30{,}000$. Using Equation (7), we can check that the results of these curve fits correspond to reasonable temperatures by comparing with the PDR temperature profiles in Figure 2 of Adams et al. (2004). This comparison shows that $T \approx 280, 640$, and 1110 K for $G_0 = 300$, 3000 and 30,000, which is consistent with the range of PDR temperatures evaluated at visual extinctions of order unity, or, equivalently, to evaluating the temperature near the base of the flow. Note however that for a given visual extinction, there is a range in the possible temperatures, depending on the gas particle density. This possible range translates into uncertainties in r_g and hence in the total mass-loss rates $\dot{M}$. More specifically, for a given FUV field strength, r_g can be higher or lower by a factor Λ, so that $r_g' = \Lambda r_g$ (where $0.5 \lesssim \Lambda \lesssim 2$). With this allowed variation, the possible change in our estimate for the total mass-loss rate can be written in terms of the ratio

$$\frac{\dot{M}'}{\dot{M}} \approx \Lambda^{3/2} e^{(1-\Lambda) r_g/2r_d} \approx \Lambda^{3/2} e^{(1-\Lambda)} , \tag{14}$$

where we have assumed that the parameter A does not change appreciably with r_g; for the second approximate equality, we assume that the typical disk radius is half the critical radius. For the range $0.5 \lesssim \Lambda \lesssim 2$, the bounds of $\dot{M}'/\dot{M}$ can be estimated from graphical analysis, and we find that $0.5 \lesssim \dot{M}'/\dot{M} \lesssim 1.1$.

3. RESULTS

Equation (8) can be numerically integrated upon specification of the viscosity parameter β (and thus α; see Equation (5)), along with the strengths of the radiation field(s) under consideration. We employ an explicit finite-difference integration scheme using a grid of 275 logarithmically spaced points, with an inner grid boundary at $r_1 \approx 0.05$ AU, and a large outer boundary $r_{\rm max} \approx 50{,}000$ AU (the grid boundary is thus much larger than the disks themselves). To ensure accurate results, we first ran simulations with all the sink terms set to zero (i.e., purely viscous evolution) and checked that the numerical results agreed with the known analytic solution (Lynden-Bell & Pringle 1974). As an additional accuracy check, we also monitored the total angular momentum of the disk, which is conserved provided that the total mass lost at the innermost grid point is included.

We fix the host star mass at $M_* = 1\, M_\odot$ and focus on an initial disk mass $M_d = 0.1\, M_*$. This star–disk mass ratio is roughly the largest that can occur without gravitational fragmentation of the disk (Gammie 2001; Shu et al. 1990). Since one of the goals of this paper is to calculate disk lifetimes in the presence of radiation fields, this star–disk mass ratio will yield an upper limit on disk lifetimes. We choose $\alpha = 10^{-3}$ and $G_0 = 3000$ as the center of parameter space, but explore wide ranges of both parameters, typically $10^{-4} \leqslant \alpha \leqslant 10^{-2}$ and $300 \leqslant G_0 \leqslant 30{,}000$. Recall that in this formulation, the parameter β in Equation (5) determines the overall viscosity of the disk, which depends on the disk midplane temperature T_m at a distance $r = 1$ AU. The disk evolution is relatively insensitive to the choice of T_m, and we fix this characteristic temperature at $T_m = 300$ K. For the purposes of this discussion, uncertainties in this characteristic temperature are equivalent to uncertainties in α.

With the viscosity parameter α, the radiation intensity G_0, and the initial surface density profile specified, Equation (8) can be integrated to solve for the surface density profile of the disk as a function of time. We also consider other quantities of interest, including the total disk mass, the outer disk radius, the mass-loss rates due to photoevaporation, and the mass accretion rate onto the star. Simulations are terminated after one of the following criteria is met: (1) the disk has lost 99% of its original mass so that it has effectively been dispersed, or (2) more than 10 Myr have elapsed.

3.1. Evaporation Due to FUV Radiation Fields from External Stars

To begin, we focus on the effects of FUV radiation from external stars (and postpone the discussion of internal radiation fields until the next section). To assess the effects of this radiation on the disk evolution, we compare our results to a reference system with purely viscous evolution (i.e., no additional radiation fields, so that the sink terms in Equation (8) are set to zero). The surface density profile is shown in Figure 2, where standard values of the parameter space have been chosen to illustrate the basic disk evolution ($\alpha = 10^{-3}$ and $G_0 = 3000$). The disk spreads on a timescale that depends on radius and is determined by the viscosity parameter. As discussed in the

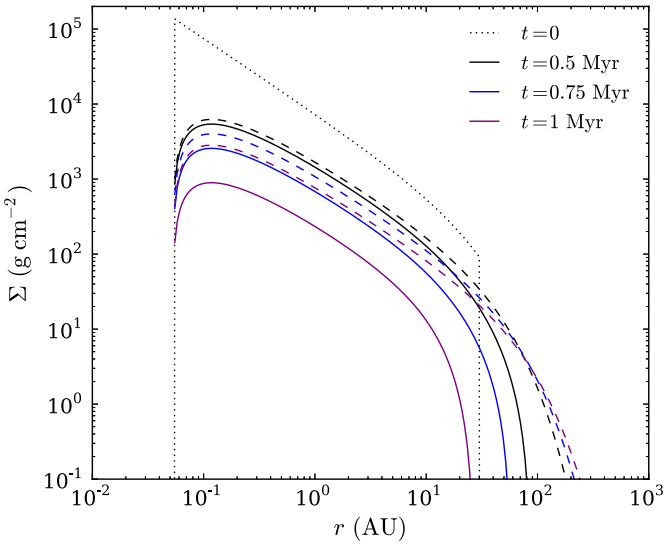

Figure 2. Surface density profile for three distinct times, as labeled, with viscosity parameter $\alpha = 10^{-3}$. The solid curves show the disk immersed in an external FUV radiation field with strength $G_0 = 3000$, and the dashed curves show purely viscous evolution (for comparison). The initial surface density profile is also shown (given by Equation (6)). For all the systems in this paper, the initial disk mass and radius are $M_d = 0.1\,M_\odot$ and $r_d = 30$ AU, respectively. The initial surface density profile has discontinuities at both the inner boundary ($r = 0.05$ AU) and at the initial outer radius ($r = 30$ AU), but these discontinuities are quickly erased as the disk diffuses.

(A color version of this figure is available in the online journal.)

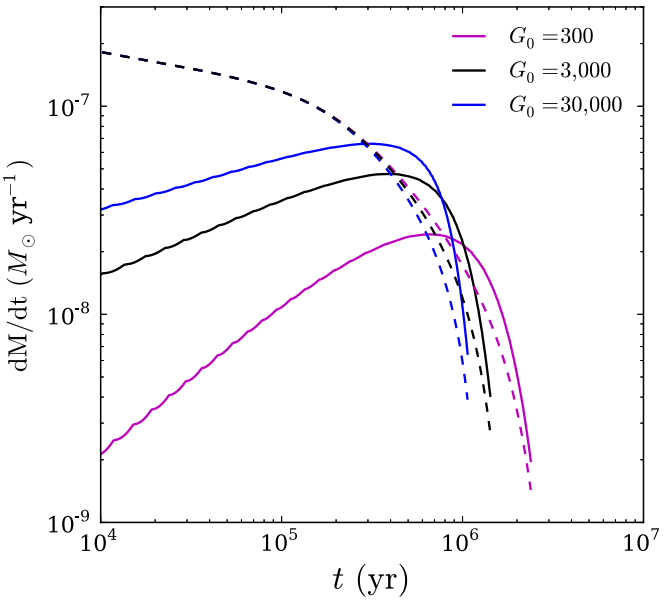

Figure 3. Mass-loss rate as a function of time due to photoevaporation (solid curves) along with the mass accretion rate onto the star (dashed curves). These results were obtained for viscosity parameter $\alpha = 10^{-3}$. For each value of the field strength G_0, the mass-loss rate is initially relatively small, and steadily increases as mass is transported outward toward regions of the disk where it can escape. The disk eventually reaches a steady state, where the time scale for mass loss is comparable to the viscous timescale.

(A color version of this figure is available in the online journal.)

previous section, the disk evolution is affected most at large radii ($r \gtrsim r_g \sim 100$ AU). The main effect of this illumination by FUV photons is to truncate the outer disk edge relative to the standard α-disk solution. However, radiation affects the disk in other ways, especially by decreasing the overall surface density after a significant fraction of the initial disk mass has been lost. Compared to the reference system, which decreases exponentially at large radii, the surface densities of disks exposed to FUV radiation decrease faster than an exponential, and thus have more sharply defined edges.

Figure 3 shows the mass-loss rate $\dot{M}$ through time for disks with $\alpha = 10^{-3}$ and FUV fluxes $G_0 = 300$, 3000, and 30,000. The solid curves show the mass loss from photoevaporation and the dashed curves show the usual mass accretion rate onto the host star. At early times, the mass loss due to photoevaporation is relatively low because the disk is compact (recall that at $t = 0$, we have chosen $r_d = 30$ AU $\ll r_g$). As the disk diffuses outward, the mass-loss rate steadily increases, reaches a peak, and then decreases again. Eventually, the time scale for mass loss due to photoevaporation is comparable to the time scale for viscous evolution, and the system reaches a steady state, where mass is steadily evaporated as it is transported to the outer portions of the disk. As expected, the mass-loss rates induced through photoevaporation depend sensitively on the strength of the external radiation field; the mass accretion rate does not show this dependence, however, because the inner portions of the disk are well shielded from the effects of the external radiation fields.

In comparison to the case of isolated systems, the lifetimes of externally illuminated disks can be drastically shortened. For the particular disk shown in Figure 2, most of the mass has been lost after ~1 Myr, through both photoevaporation and accretion onto the star. At first glance, one might expect the disk lifetime to be determined primarily by the radiation field strength G_0. In practice, however, the disk lifetime is intimately linked to the relative strengths of G_0 and the viscosity parameter α. For any radiation intensity, significant mass loss cannot occur unless the disk expands enough so that mass reaches the outer (shallower) portions of the gravitational potential well of the host star; when this condition is met, the gas can freely escape. Thus, for efficient mass loss, externally illuminated disks must have sufficiently high viscosity to cause enough mass to be transferred outward where it can become unbound. Figure 4 shows the total disk mass as a function of time for $\alpha = 10^{-4}$, 10^{-3}, and $10^{-2,}$, and $G_0 = 300$, 3000, and 30,000. Disks with high viscosity ($\alpha = 10^{-2}$) are effectively dispersed in less than 0.5 Myr; disks with low viscosity ($\alpha = 10^{-4}$) live for at least 5 Myr, and, for low FUV flux ($G_0 = 300$), can survive for longer than 10 Myr. Note that numerical estimates of α based on magneto-rotational instability (MRI) simulations yield values in the range $\alpha \sim 10^{-3}$–10^{-2} (e.g., Brandenburg et al. 1996). These results imply that long-lived disks should not be common in populated star-forming regions.

In the absence of external radiation fields, the outer disk edge increases with time as a power-law (and has no upper bound). Note that the term "outer disk edge" itself is somewhat ambiguous, because the standard α-disk solution for the surface density decreases exponentially at large radii, and thus does not have a clearly defined outer boundary. In order to get an estimate for the degree to which the disk is truncated, we define r_d (where r_d is a function of time) as the radius where the enclosed mass is some critical fraction of the total mass, i.e.,

$$M_{\rm enc}(r_d, t) = \int_{r_1}^{r_d} 2\pi r \Sigma\, dr = f\, M_d(t) = f \int_{r_1}^{\infty} 2\pi r \Sigma\, dr. \quad (15)$$

Since the choice of the critical fraction f is somewhat arbitrary, we consider several values to ensure that the qualitative behavior of $r_d(t)$ does not depend sensitively on the particular choice of f. Figure 5 shows the results for $f = 0.75$, 0.95, 0.99, and 0.999.

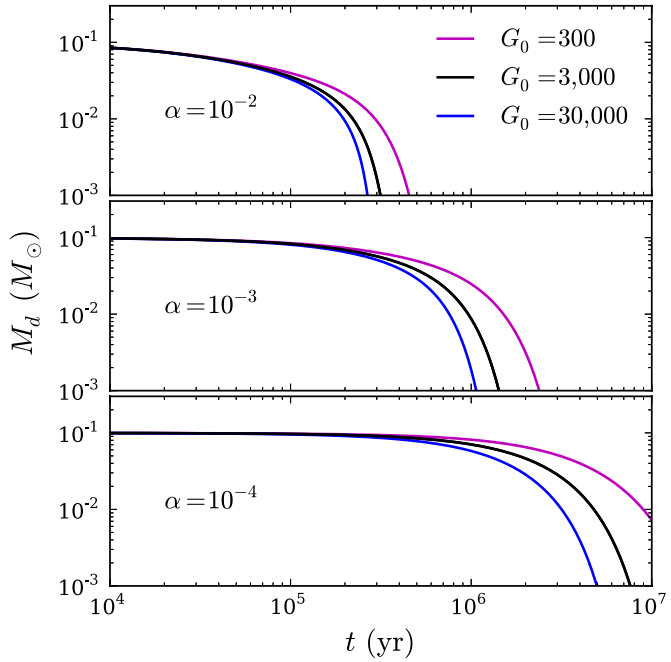

Figure 4. Disk mass as a function of time for three values of α and G_0, as labeled. Disks with high viscosity ($\alpha = 10^{-2}$, top panel) evolve quickly and are depleted within 0.5 Myr. Disks with moderate viscosity ($\alpha = 10^{-3}$, middle panel) evolve more slowly and survive somewhat longer, but are nonetheless dispersed in less than ∼2.5 Myr. Disks with low viscosity ($\alpha = 10^{-4}$, bottom panel) diffuse more gradually and can survive for at least 5 Myr, and even longer than 10 Myr if the external field strength is relatively low.

(A color version of this figure is available in the online journal.)

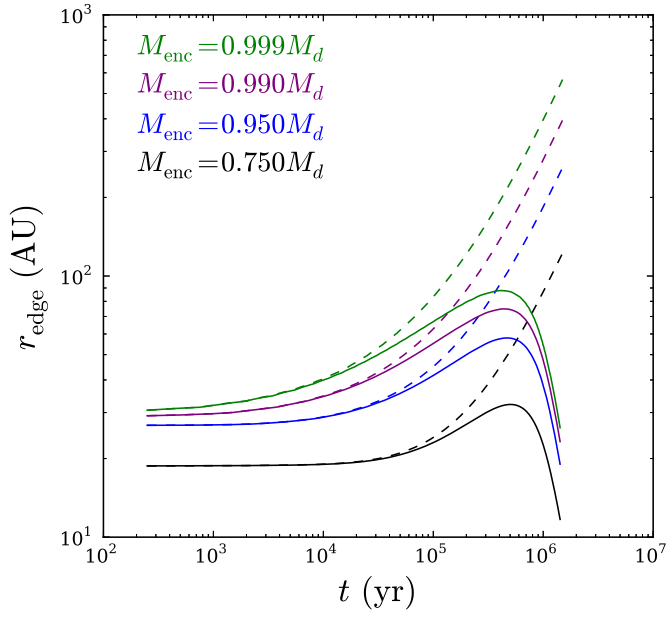

Figure 5. Radius of our "standard" photoevaporating disk ($G_0 = 3000$, $\alpha = 10^{-3}$) as a function of time (solid curves), along with the results for a purely viscously evolving disk (dashed curves). Each color corresponds to a different choice for the critical fraction f used to define the outer disk edge (see Equation (15)), as labeled. The similar behavior of each curve suggests that the choice of f in defining the disk edge is not particularly important; for the remainder of this paper, we adopt a value $f = 0.99$.

(A color version of this figure is available in the online journal.)

Since the shape of the curves is similar for all four cases, we can safely fix the critical fraction to be $f = 0.99$ for the remainder of this paper. This choice yields uncertainties in the disk edge of order 10% (where this uncertainty is due to the definition of

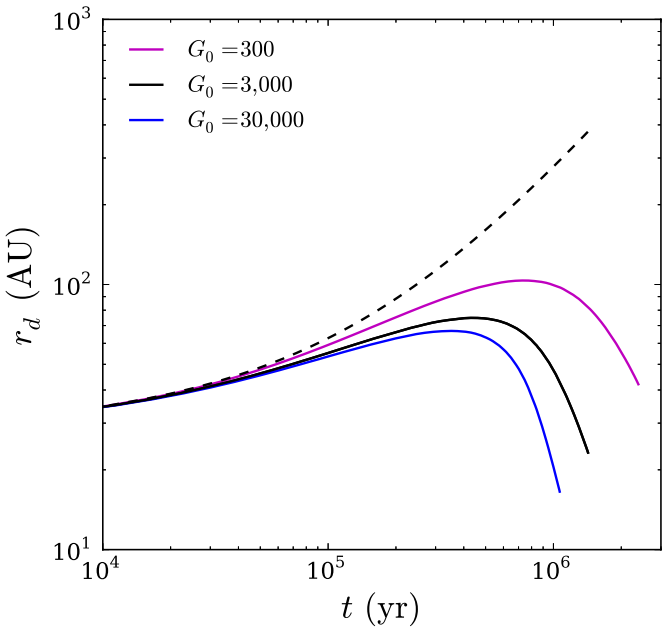

Figure 6. Disk radius as a function of time for $\alpha = 10^{-3}$, and for radiation fields $G_0 = 300$ (top magenta solid curve), $G_0 = 3000$ (middle black solid curve), and $G_0 = 30{,}000$ (bottom blue solid curve). The dashed curve, included for comparison, shows the radius for a disk with no evaporation. The contrast between the power-law behavior of the dashed curve and the three solid curves illustrates the truncation effects of the radiation fields. The solid curves (with evaporation) are initially smoothly increasing because the viscous time scale is greater than the mass-loss time scale; mass is thus transported outward faster than it can be evaporated. As the disk diffusion slows, mass is steadily evaporated as it travels outward, and the disk radius begins to decrease.

(A color version of this figure is available in the online journal.)

what we mean by the disk edge, and is not due to inaccuracies in determining disk surface density profiles). Figure 6 shows the disk edge r_d as a function of time for three values of G_0 and with fixed viscosity ($\alpha = 10^{-3}$). Initially, the disk expands faster than it can be evaporated. As the viscous time scale slows at later times, however, mass in the outer disk becomes unbound as soon as it is transported outwards, and the radius starts to decrease with time. In all cases that include photoevaporation, after ∼0.5 Myr have passed, the disk radii are noticeably smaller than they would be in the absence of external radiation. At longer times, ∼1–2 Myr, the disk radii become smaller than their initial size. For this particular set of parameters, the disk edge never increases beyond $r_d \approx 100$ AU. Figure 7 shows the same results for different viscosities. The behavior is qualitatively similar for all parameters. Disks with the highest viscosities have the largest maximum radii, but are dispersed on the shortest time scales.

A potentially important parameter in these calculations is the initial outer disk radius $r_d(0)$, because the extent of the disk determines the mass loss due to evaporation (from Equation (9)). Since our model focuses on the subcritical regime, the discussion is restricted to initial radii less than the escape radius $r_g \sim 100$ AU. We repeated our calculations using $r_d(0) = 15$ and 60 AU, i.e., within factors of two of our standard value $r_d(0) = 30$ AU. The resulting mass-loss rates, radii, and masses are shown in Figure 8. The disk mass as a function of time is almost completely independent of the initial disk radius, and the mass-loss rate and disk edge converge to nearly the same value after ∼0.5 Myr have elapsed. Note that disks with the smallest radii are depleted the most quickly, in spite of the fact that the

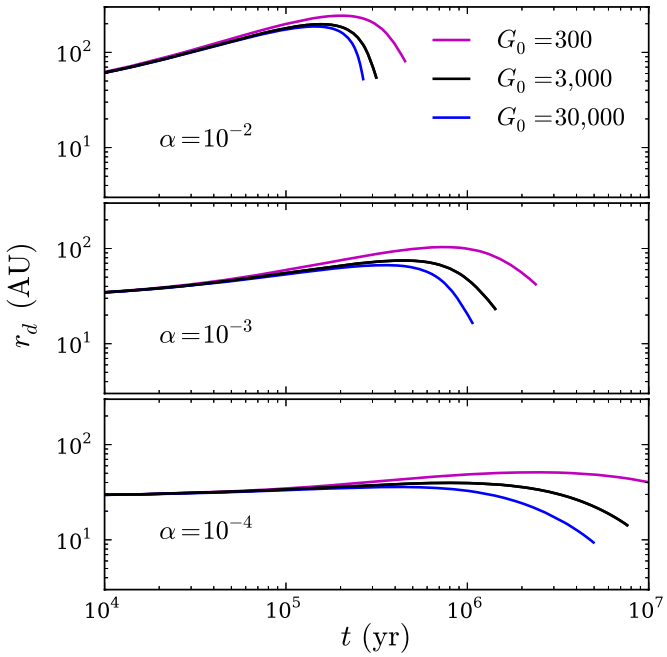

Figure 7. Disk radius as a function of time (as in Figure 6) for three values of the viscosity parameter α and three values of the external radiation field G_0, as labeled.

(A color version of this figure is available in the online journal.)

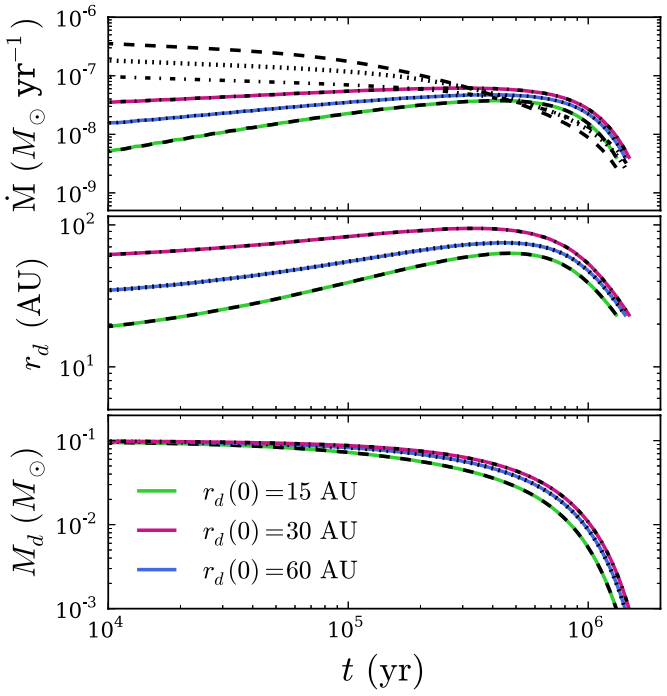

Figure 8. Mass-loss rate, disk radius, and disk mass through time for our standard parameters $G_0 = 3000$ and $\alpha = 10^{-3}$, illustrating the effects of changing the initial radius $r_d(0)$. The colored curves correspond to the mass loss due to photoevaporation for differing values of the starting radius, as labeled. In the top panel, the black dashed, dotted, and dash-dotted curves (from top to bottom) show the mass accretion rate onto the host star for initial radius $r_d(0) =$ 15, 30, and 60 AU respectively. Note that although the disk mass through time is almost independent of the initial radius, disks with the smallest initial radii are dispersed on slightly shorter time scales, because the mass accretion rate early in the disk evolution is the highest.

(A color version of this figure is available in the online journal.)

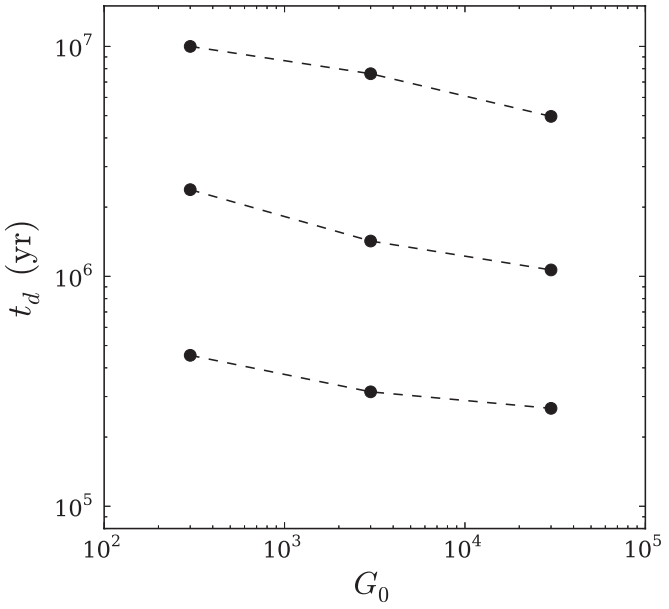

Figure 9. Disk lifetime t_d as a function of G_0 for $\alpha = 10^{-2}$, 10^{-3}, and 10^{-4} (from bottom to top). We define t_d to be the time needed for a disk to lose 99% of its original mass (if t_d exceeds 10 Myr, however, we terminate the simulation, and set $t_d = 10$ Myr to get a lower bound). For a given G_0, there is a range of disk lifetimes t_d, which depend on the value of α; this range spans over an order of magnitude, and shows the importance of not only the strength of the radiation field, but also the amount of viscosity in the disk. Notice that nearly all disks are dispersed before 10 Myr have passed, and many in less than 2–3 Myr.

photoevaporative mass loss is decreased (since less material is located in the outer regions where it can escape). This trend arises because the mass accretion rate is initially highest for disks with the smallest radii. The main conclusion that can be drawn from Figure 8 is that the initial disk radius is relatively unimportant in the long-term evolution.

We can summarize our main results by plotting the disk lifetime t_d as a function of the radiation field strength G_0 (for each value of α), as shown in Figure 9. The figure shows that for fixed G_0, there exists a wide range of possible disk lifetimes (spanning over an order of magnitude) depending on the viscosity. This result highlights the importance of the viscosity to disk dispersal. Regardless of the radiation field strength, disks with low viscosity ($\alpha \leqslant 10^{-4}$) can survive for relatively long spans of time, essentially because mass is transported outward slowly. Nonetheless, notice that nearly all of the disks are destroyed before 10 Myr have elapsed. Furthermore, for expected viscosities (with $\alpha \gtrsim 10^{-3}$), the disk mass is depleted on rapid time scales $t_d \lesssim 2.5$ Myr. These results show that external FUV radiation fields can be important in disk dispersal, and imply that disks with ages $t_d \gtrsim 3$ Myr should be rare or nonexistent within richly populated clusters.

3.2. Combined Effects of External FUV and Internal X-Ray Fields

Given the results of the previous section, the next step is to include photoevaporation due to radiation from the host star. In particular, we want to identify the relative importance of internal and external radiation fields, for varying choices of the other relevant parameters. Owen et al. (2012) showed that out of the EUV, FUV, and X-ray radiation fields generated by the host star, the X-rays are often the dominant agent for disk dispersal. As a result, we neglect FUV and EUV radiation fields for this current assessment and consider only X-rays. To model this

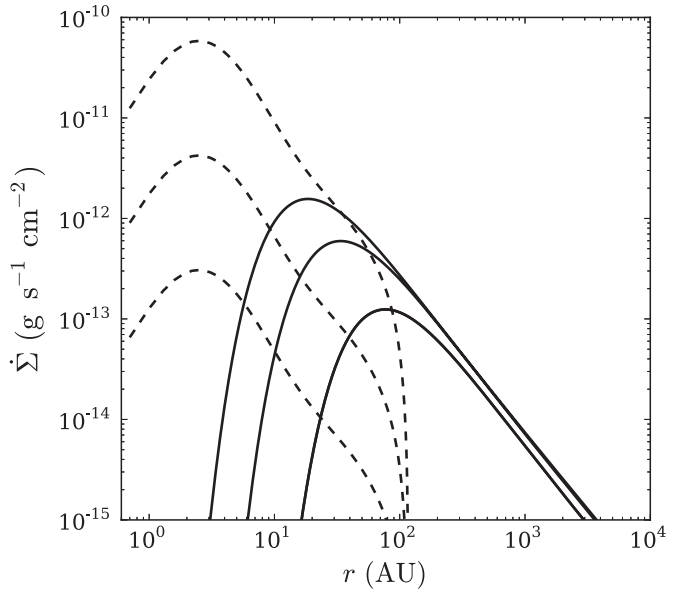

Figure 10. Radial dependence of the sink terms $\dot{\Sigma}$. The solid curves represent the analytic approximation for photoevaporation from external stars (Equation (13)), taken from Adams et al. (2004), normalized to flux levels $G_0 = 300$, 3000, and 30,000 (bottom to top). The dashed curves show the numerical fits for X-ray evaporation from the host star, given by Owen et al. (2012). The dashed curves are normalized to X-ray luminosities $L_X = 10^{29}$, 10^{30}, and 10^{31} erg s^{-1} (bottom to top).

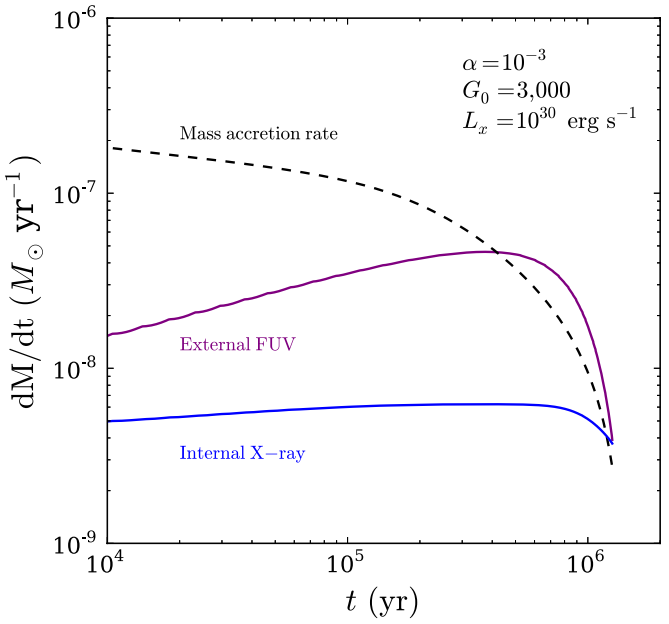

Figure 11. Mass-loss rates as functions of time, similar to those shown in Figure 3, but with the inclusion of photoevaporation due to X-rays from the host star. The X-ray luminosity is $L_X = 10^{30}$ erg s^{-1} and the external FUV radiation field has $G_0 = 3000$.

(A color version of this figure is available in the online journal.)

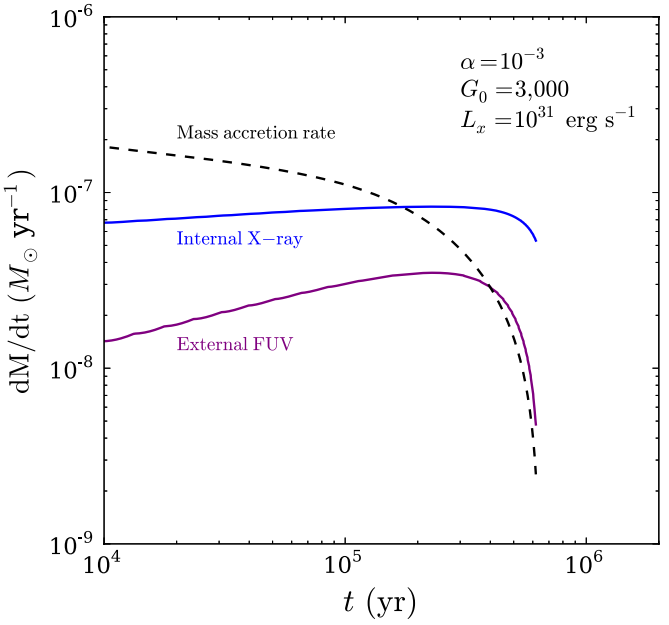

Figure 12. Mass-loss rates as functions of time, similar to those shown in Figure 11, but with $L_X = 10^{31}$ erg s^{-1}. For this larger value of the X-ray luminosity, the mass-loss rate due to internal radiation $\dot{M}_x$ exceeds that due to external radiation $\dot{M}_{\rm FUV}$ for all phases of disk evolution (compare with Figure 11).

(A color version of this figure is available in the online journal.)

X-ray photoevaporation, we use the numerical fits for $\dot{\Sigma}$ provided by Owen et al. (2012, see Appendix B, Equation (B2)). Figure 10 shows the radial dependence of the mass-loss profile, normalized to X-ray luminosities $L_X = 10^{29}, 10^{30}, 10^{31}$ erg s^{-1} (dashed curves), along with the analytic prediction for the mass-loss profile for external FUV (Equation (13)), normalized to $G_0 = 300$, 3000, 30,000 (solid curves).

To start we fix the X-ray luminosity at $L_X = 10^{30}$ erg s^{-1} and look at its effects on our standard disk with $\alpha = 10^{-3}$ and $G_0 = 3000$. Figure 11 shows the mass-loss rates due to each source, $\dot{M}_{\rm FUV}$ and $\dot{M}_X$, along with the mass accretion rate. Unlike the mass-loss rate $\dot{M}_{\rm FUV}$ due to external FUV radiation, the internal contribution $\dot{M}_X$ does not increase considerably with time as the disk spreads. The penetration of X-rays from the host star is mostly confined to inner regions of the disk (near the star), where a plentiful mass supply exists at the start of the simulations. Nonetheless, mass loss from X-rays increases slowly as the disk spreads, so that a larger area of the disk can evaporate (see the profiles in Figure 10). At late times, the disk radius shrinks, so that the mass loss from X-rays decreases.

For the same disk and an elevated X-ray luminosity $L_X = 10^{31}$ erg s^{-1} (i.e., a factor of 10 higher), the mass-loss rates are shown in Figure 12. Note that this value for L_X represents the upper end of the possible range in X-ray luminosity for a solar-mass star (Flaccomio et al. 2012; Güdel et al. 2007), thereby giving an estimate of the maximum possible effects of X-ray fields. The figure shows that this increase in luminosity causes the mass loss from X-ray evaporation to exceed that from external FUV fields; internal radiation is thus important for this portion of parameter space. Nonetheless, nearly all solar-type stars have X-ray luminosities somewhat lower than $L_X = 10^{31}$ erg s^{-1} (e.g., see the X-ray luminosity functions in Wang et al. 2008). As a result, for disks in sufficiently populated clusters, we conclude that the dominant agent for mass loss will generally be the external radiation fields.

Figure 13 presents the time evolution for the disk mass and disk radius for the varying strengths of the internal radiation fields (determined by L_X) and external radiation fields (determined by G_0). The effect of adding an X-ray contribution from the host star with luminosity $L_X = 10^{30}$ erg s^{-1} to an external FUV field is negligible, which is consistent with Figures 11 and 12. Evaporation from host stars with X-ray luminosities $L_X \leqslant 10^{30}$ erg s^{-1} is therefore secondary in importance to

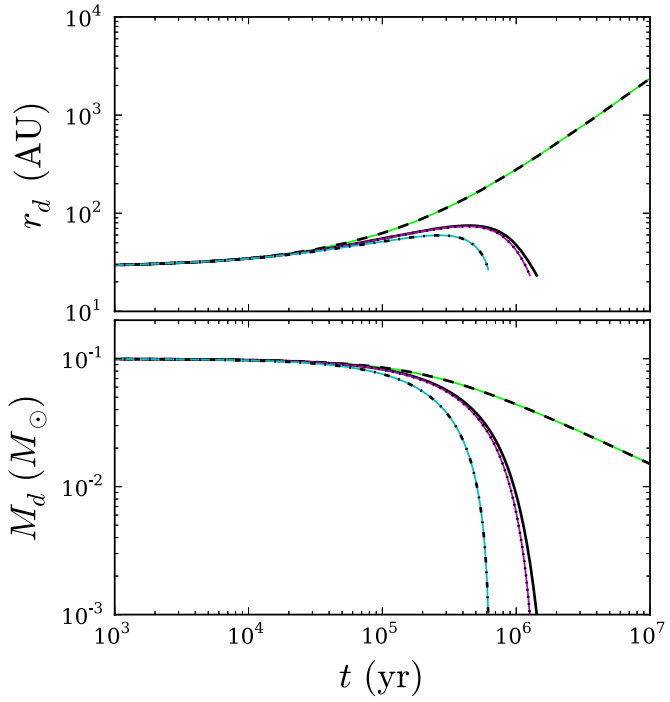

Figure 13. Disk radius (top panel) and mass (bottom panel) as functions of time for varying contributions from internal and external radiation fields. All curves correspond to viscosity parameter $\alpha = 10^{-3}$. Green dashed curve shows results for a disk with no photoevaporation; solid black curve corresponds to radiation fields $G_0 = 3000$ and $L_X = 0$; magenta dotted curve corresponds to radiation fields $G_0 = 3000$ and $L_X = 10^{30}$ erg s^{-1}; and finally the cyan dash-dot curve shows results for $G_0 = 3000$ and $L_X = 10^{31}$ erg s^{-1}. Notice that the solid black and magenta dotted curves are nearly identical, i.e., an X-ray luminosity $L_X = 10^{30}$ erg s^{-1} does not significantly influence disk evolution when coupled with an external FUV field. However, increasing the luminosity to $L_X = 10^{31}$ erg s^{-1} shortens the disk lifetime by nearly a factor of two.

(A color version of this figure is available in the online journal.)

evaporation by external FUV fields. Increasing the X-ray luminosity to $L_X = 10^{31}$ erg s^{-1}, which represents the upper end of the observed range, shortens the disk lifetime by nearly a factor of two.

The discussion thus far has ignored the spectrum of the X-rays irradiating the disk. For completeness we note that as the X-ray luminosity increases over its expected range ($L_X = 10^{29}$–10^{31} erg s^{-1}), the spectra are observed to become harder, and can have a strongly penetrating ultrahard component during some flares (Preibisch et al. 2005; Getman et al. 2008).

3.3. Comparison with Observed Proplyds in the Orion Nebula Cluster

Next we test the previous developments by comparing the model predictions with observed disks in the ONC. These objects (often called the proplyds) are illuminated by radiation from the four massive Trapezium stars, most notably θ^1 Ori C, a 40 $M_\odot$ O star near the cluster center. Disks residing within ~2 pc of the center are sufficiently illuminated so that the results of this paper are applicable (but the observed proplyds have much smaller projected distances). Since the cluster radius is estimated to be $r_c \approx 2.5$ pc (Hillenbrand & Hartmann 1998), the entire population of disks in the cluster is potentially exposed to strong radiation fields.

In this section, for the sake of definiteness, we consider only external irradiation from FUV sources and neglect the effects of X-rays from the host star. Using results from our model, including both viscous evolution and external evaporation due to FUV radiation, we construct "evolutionary tracks" in the mass–radius plane. Any given disk must have a mass M_d and r_d at any given time, and our model predicts the locus of points traced out in the (r_d, M_d) plane as the system evolves. We can then compare these tracks with observational data. Vicente & Alves (2005) present diameters for 144 disks in the ONC. Some diameters were measured by observing the dark silhouette of the disk against the bright background (denoted hereafter as the "silhouette disks"), but most were inferred by measuring the light from their own ionization fronts (IFs) caused by the hot Trapezium stars (hereafter the "IF disks"). The diameter of the IF is somewhat larger than the true disk diameter; Vicente & Alves (2005) attempted to correct for this effect, and estimated that the IF diameter is approximately twice the disk diameter. Their estimated measurement errors of the IF diameters are ~20 AU; however, the uncertainties in the disk diameters are somewhat larger, because of uncertainties in the relationship between the IF and the disk edge. Note that their data set does not contain any disks with radius $r_d < 30$ AU because such small disks were below their resolution limit. Disk masses for a subset of this sample have been measured by Mann & Williams (2010) based on observations of their sub-millimeter flux. Calculating disk masses in this manner requires assumptions about the dust opacity, the gas to dust ratio, and the distance to the cluster (see, for example, Williams & Cieza 2011); these assumptions lead to uncertainties in the disk masses. Together, the two data sets yield a sample of 28 disk systems in the ONC with both measured masses and radii. Mann & Williams (2010) also present upper limits on disk masses for an additional 25 disks; including this latter set of disks, the sample size increases to 53.

Figure 14 compares the predictions of our model with observed disk systems, where each panel shows a different value of the external radiation field G_0 (from 300 to 30,000). In each panel, the bold solid curves show the disk evolution through time for viscosity parameters $\alpha = 10^{-4}$ (left), $\alpha = 10^{-3}$ (middle), and $\alpha = 10^{-2}$ (right). Note that the evolutionary tracks are only plotted here for $t \leqslant 2$ Myr, because the observed disks in the ONC are estimated to have ages of order 2 Myr or less. As a result, the tracks for the lowest α values are truncated (since disks with low viscosity evolve very slowly). The dotted curves connecting the solid curves are "isochrones," i.e., curves corresponding to constant values of time, but with varying sizes of the viscosity parameter; here we have chosen viscosity parameters in the range $10^{-4} \leqslant \alpha \leqslant 10^{-2}$ to represent the approximate bounds of the parameter space. The isochrones (shown as dotted curves) mark evolutionary times of $t = 0.25$, 0.5, 1.0, 1.5, and 2 Myr (from top to bottom). The blue data points show the 28 disks with estimated masses, and the green points show the 25 disks with upper limits on their masses. Triangles denote the silhouette disks, while squares and circles indicate the IF disks. As we argue below, these models are consistent with disk ages that fall in the range $0.25 \lesssim t_d \lesssim 1.0$ Myr.

In general, the mass–radius data for observed disks are nicely bounded by the "edges" of the expected parameter space. Essentially all of the points in Figure 14 are contained within the region predicted for viscosity parameters in the range $\alpha = 10^{-4}$–10^{-2}, radiation fields in the range $G_0 = 300$–30,000, and times $t < 2$ Myr. Furthermore, the best agreement between the model and observations occurs for relatively intense radiation fields with $G_0 = 3000$ or 30,000. This finding is sensible, given that the disks reside in an environment (the ONC) containing

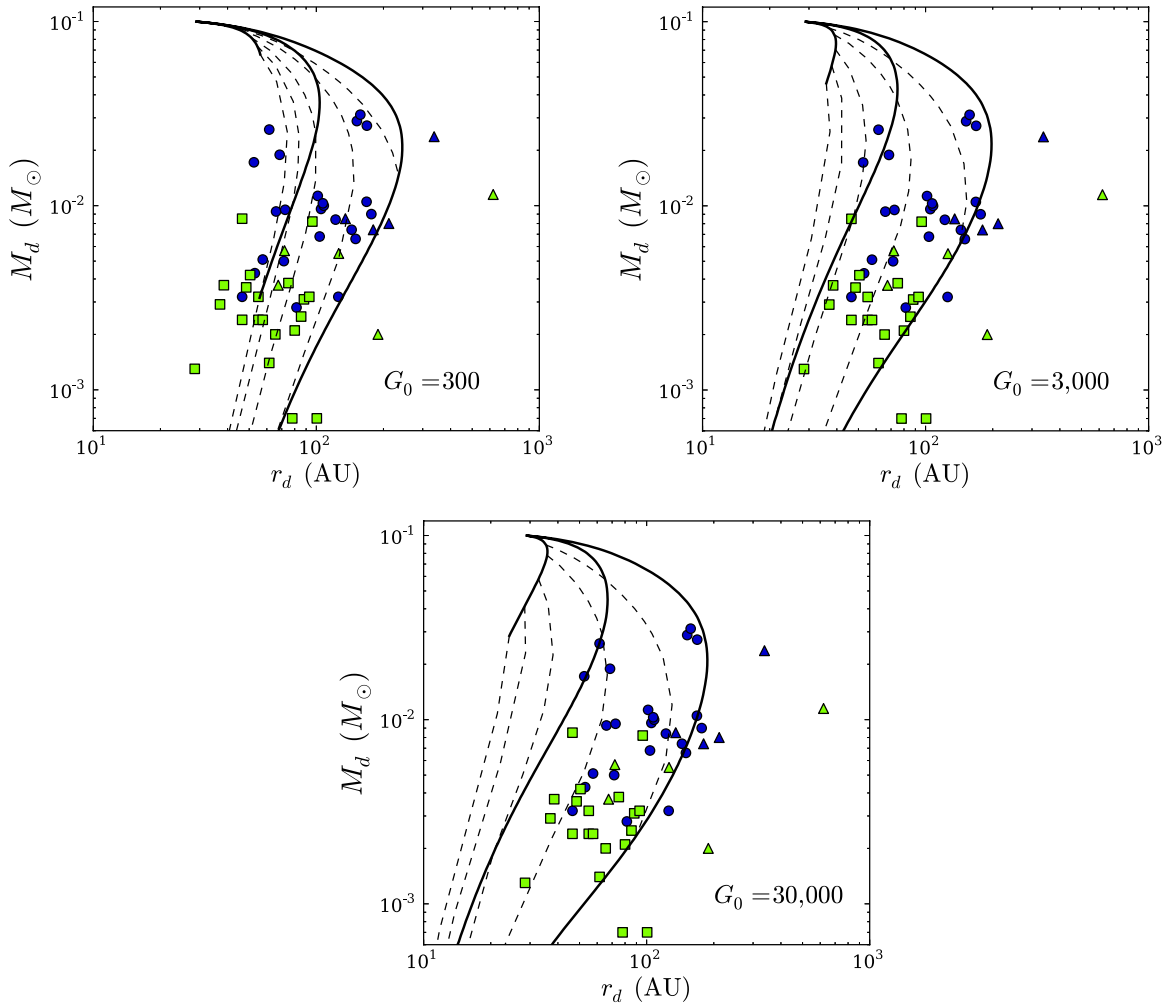

Figure 14. "Evolutionary tracks" (solid curves) and "isochrones" (dotted curves) in the plane of disk mass and radius (r_d, M_d), along with observational data for disks in the Orion Nebula Cluster. The disk masses are taken from Mann & Williams (2010) and radii from Vicente & Alves (2005). Dark blue points show disks with measured masses, light green points show data with mass upper limits. The triangles indicate silhouette disks, whereas circles and squares indicate ionization front disks (see text). Each panel shows a different value of G_0, as indicated. All of the evolutionary tracks start at the point (r_d, M_d) = (30, 0.1) at $t = 0$ and travel downward in time. These evolutionary tracks are limited to times $t \leqslant 2$ Myr, to be consistent with the inferred age of the ONC. In each panel, the three solid curves show the disk evolution for different viscosities, with $\alpha = 10^{-4}$ (left), $\alpha = 10^{-3}$ (middle), and $\alpha = 10^{-2}$ (right). The dotted curves are isochrones, i.e., points at fixed times, with times $t = 0.25$, 0.5, 1.0, 1.5, and 2 Myr (from top to bottom).

(A color version of this figure is available in the online journal.)

many massive stars. Data points that fall outside of the model predictions include many of the silhouette disks (marked by triangles). This result is not unexpected, because the silhouette disks are, on average, farther from the cluster center, where the radiation fields are weaker (and where larger disks can survive). Note that there is a degeneracy in the predicted disk mass and radius of our model; at a given time, multiple combinations of α and G_0 can yield the same mass and radius. As a result, we cannot unambiguously predict the expected parameters for a particular observed disk. However, the range of parameters for which the best agreement occurs is reasonable: Figure 14 indicates that most of the data points can be understood using a limited range of parameter space, with a preference for viscosity parameters $10^{-3} \leqslant \alpha \leqslant 10^{-2}$, and radiation fields with $G_0 =$ 3000 or 30,000. This range of α values is predicted by many MRI simulations (e.g., Brandenburg et al. 1996), and this range of G_0 values is typical for young clusters (Fatuzzo & Adams 2008; Holden et al. 2011). To move forward, we need to break the degeneracy between the α and G_0 values, which requires additional information; for example, it would be useful to find the true distance of a disk from the cluster center (rather than projected distance).

The results shown in Figure 14 are based on a single initial disk radius $r_d = 30$ AU. In practice, however, young disks will display a range of radii, where the value depends on the initial angular momentum and its evolutionary history. To explore the effects of varying initial disk sizes, we have repeated these calculations for initial radii $r_d = 15$ and $r_d = 60$ AU, i.e., varying the disk radius by a factor of two in both directions (see Section 3.1 and Figure 8). The resulting evolutionary plots (not shown) are nearly identical to those in Figure 14. This finding demonstrates that disk properties (as a function of time) are relatively insensitive to the initial disk radius, in agreement with previous work (Clarke 2007), as well as the results shown in Figure 8.

Although the true distances of individual disks from the cluster center in three-dimensional space cannot be inferred with current data, we can estimate the expected distribution of distances (and hence FUV fluxes) for the entire sample. Denoting the true distance as r and the projected distance as d_p,

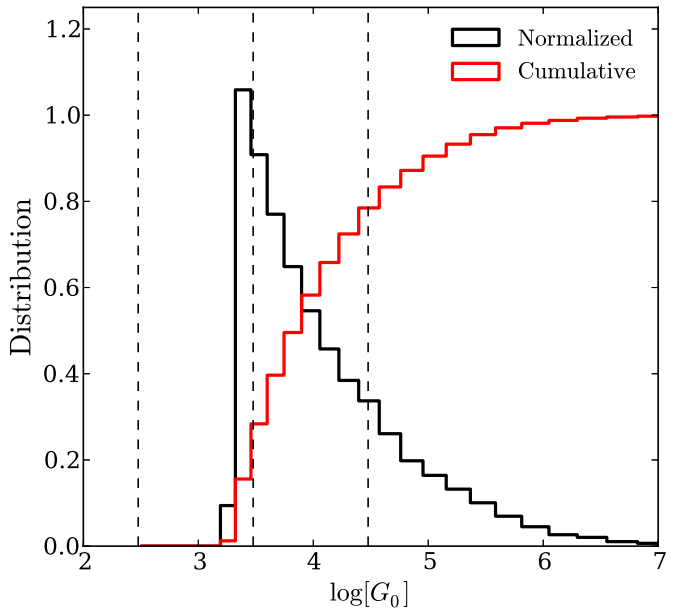

Figure 15. Distribution of expected FUV fluxes based on the 28 disks in the ONC with measured masses and radii (denoted by blue data points in Figure 14). Note that the scale for the x-axis uses common logarithms. For each disk with projected distance d_p from the cluster center, the line-of-sight distance s was randomly sampled $N_s = 10^5$ times. For reference, the figure includes benchmark values (marked by vertical dashed lines) for the three FUV fluxes explored in this paper, i.e., $G_0 = 300$ (left), 3000 (middle), and 30,000 (right). No disks are exposed to flux levels $G_0 < 2000$ because of our estimate for $L_{\rm FUV}$, and because all disks are assumed to be located within $r \leqslant 2.5$ pc of the cluster center. The peak of the distribution occurs near $G_0 \approx 3000$, consistent with our previous assumptions.

(A color version of this figure is available in the online journal.)

the (hidden) line-of-sight distance s is given by the expression

$$r^2 = d_p^2 + s^2 \,. \tag{16}$$

Here, we allow the line-of-sight distance s to be uniformly sampled within the range

$$0 \leqslant s \leqslant r_c \sqrt{1 - d_p^2 / r_c^2}, \tag{17}$$

where r_c is the cluster radius. Vicente & Alves (2005) provide projected angular distances for their sample of disks; we convert these measurements to linear projected distances by assuming a distance to the ONC of 414 pc (Menten et al. 2007). We then set the cluster radius $r_c = 2.5$ pc (Hillenbrand & Hartmann 1998), and repeatedly sample s for each observed disk in the range given by Equation (17). The dimensionless FUV flux then takes the form

$$G_0 = \frac{1}{F_0} \frac{L_{\rm FUV}}{4\pi \left(d_p^2 + s^2 \right)}, \tag{18}$$

with the typical interstellar flux level $F_0 = 1.6 \times 10^{-3}$ erg s^{-1} cm^{-2} (Habing 1968). A cluster like the ONC consisting of $N \sim 2000$ stars is expected to have an FUV luminosity $L_{\rm FUV} \approx 2.46 \times 10^{39}$ erg s^{-1} (Fatuzzo & Adams 2008).

The results of this analysis are shown in Figure 15, where the random variable s (from Equation (17)) has been uniformly sampled $N_s = 10^5$ times for each of the 28 disks with measured masses and radii (corresponding to the blue data points in Figure 14). Nearly 80% of all disks in this distribution have flux levels of $G_0 \leqslant 30{,}000$, indicated by the rightmost vertical dashed line. No disks in this sample have flux levels below $G_0 \approx 2000$; this minimum flux occurs because all are assumed to be located within the cluster radius $r_c = 2.5$ pc. These results are consistent with the evolutionary tracks shown in Figure 14, because the best agreement between the model predictions occurs for higher FUV fluxes, those with $3000 \leqslant G_0 \leqslant 30{,}000$.

4. CONCLUSION

4.1. Summary of Results

In order to understand the effects of external stellar radiation on disk evolution, this paper has incorporated photoevaporation models (Adams et al. 2004) into time-dependent evolutionary models for the disks (using an α prescription). We use this framework to derive constraints on disk lifetimes, mass-loss rates, radii, and masses. In contrast to most previous work concerning photoevaporating disks, this paper focuses on the effects of radiation fields from external stars (but see also Armitage 2000 and Clarke 2007). We also consider photoevaporation by X-rays from the host star (Owen et al. 2012) in order to assess the relative importance of internal versus external radiation sources for evaporation. An immediate application (and test) of the model is provided by the ONC, where the entire disk population is illuminated by the Trapezium O stars, and where new data are available. Our main results can be summarized as follows.

1. Photoevaporation from external FUV sources severely reduces the disk masses, and truncates the disk radii, over most of the expected parameter space. For a given external radiation field, the most important parameter in determining the disk lifetime is the viscosity (given here by α). Disks with viscosity parameter in the range $10^{-3} \lesssim \alpha \lesssim 10^{-2}$ diffuse outward on time scales that are short enough so that disk material is continuously transported to regions of low gravitational potential where it can freely escape. Even disks exposed to moderate FUV radiation ($G_0 = 300$) can be significantly depleted on short time scales when the viscosity is sufficiently high ($\alpha \gtrsim 10^{-3}$). Disks with moderate viscosity (with $\alpha = 10^{-3}$) are effectively dispersed in 1–3 Myr; disks with higher viscosity ($\alpha = 10^{-2}$) are dispersed within ~0.5 Myr (see Figures 4 and 9). Disk sizes are quickly truncated to radii $r_d < 100$ AU over the full range of parameter space, and many disks are truncated even further, so that $r_d < 30$–50 AU (Figure 7).
2. When combined with existing X-ray photoevaporation models from the host star (Owen et al. 2012), the mass loss from external FUV radiation dominates except for host stars with the highest X-ray luminosities ($L_X = 10^{31}$ erg s^{-1}). Disk masses are usually depleted by external FUV fields before any interesting effects from the X-rays can occur, such as "holes" in the inner disk, i.e., regions where photoevaporation clears out mass faster than it can be replenished through viscous transport. This kind of structure can only emerge when the viscous time scale is comparable to the mass-loss time scale (for X-ray evaporation). Since the viscous time scale starts out relatively high, the disk must evolve for some time (typically ~4–5 Myr) before gaps can be formed by X-rays.
3. Our evolutionary model (including only FUV radiation from external stars, and excluding X-rays from the central star) is in good agreement with observed masses and radii for disks in the ONC (see Figure 14). The best agreement with the data generally occurs for relatively high radiation fields, those with $G_0 = 3000$–$30{,}000$, and for disk viscosity parameters in the range $10^{-3} \leqslant \alpha \leqslant 10^{-2}$. Figure 14 also

shows that circumstellar disks follow well-defined tracks in the plane (r_d, M_d) of disk mass and radius; such plots can thus be used to study disk evolution (analogous to the use of the H-R diagram for stellar evolution).

4.2. Discussion

The main result of this paper is that disks can be readily destroyed by strong external FUV radiation fields, sometimes within 1 Myr, often within 2–3 Myr, and nearly always within 10 Myr. For fixed initial disk masses and radii, this wide range in possible disk lifetimes is due primarily to variations in disk viscosity (α). Since the formation time scale of giant planets via core accretion is estimated to lie in the range ∼1–10 Myr (Pollack et al. 1996), the potential for planet formation in populated star-forming regions can often be suppressed. This constraint can be evaded if the viscosity is relatively low (with $\alpha \lesssim 10^{-3}$). At first glance, this result is puzzling, because most stars are thought to form in clusters rather than in isolation (Lada & Lada 2003)—and yet both single and multiple planet systems appear to be common. Furthermore, our own solar system had sufficient material from which to form planets, even though it was probably born in a relatively populated cluster (Adams 2010, and references therein).

However, it is important to remember that only a subset of young stars experience the most extreme environments considered in this paper. The regions of parameter space where planet formation is most threatened are those with FUV fluxes $G_0 \sim 30{,}000$, which generally corresponds to disks located within ∼0.1 pc of the OB star(s) generating the FUV fields (the exact number will depend on the luminosity of the FUV sources, which varies from cluster to cluster). At such close distances, planet formation is likely to be compromised unless the disk viscosity is extremely low. Most disks, however, are located at distances $r \sim 1$ pc, so they experience lower flux levels (even in populated clusters). The density profile of a star cluster can be approximated as $\rho(r) \sim r^{-2}$, so that the enclosed mass $M(r) \propto r$. As a result, most of the stars (and their disks) are located in the outer regions of the cluster, and are therefore exposed to fluxes near the lower end of the range considered in this paper. If we take $G_0 = 300$ as a typical flux value for many disks, then planet formation is probably not significantly threatened, as long as there are enough disks with viscosity parameters smaller than $\alpha = 10^{-2}$.

Another way for disk lifetimes to be extended long enough to allow planet formation is by considering the dynamical interactions of star–disk systems within clusters. Over the course of ∼1 Myr, stars can change their positions relative to the massive star(s) that are responsible for most of the radiation. If a star's orbit around the photon source is highly eccentric,[3] it will spend most of its time in the outer cluster regions with low FUV flux, and experience only brief periods of higher flux. This could potentially allow individual disks to retain their mass for somewhat longer, perhaps long enough to form planets. Considering these types of dynamics would be equivalent to introducing a time-dependent G_0 into our model. Note however that if the field strength never falls below $G_0 \sim 300$ over an orbit, then the results of this paper imply that dynamical interactions can probably only extend disk lifetimes by a factor of two or so.

[3] Note that describing orbits as "eccentric" here is somewhat misleading, or at least requires further specification, because the gravitational potential of the cluster is not Keplerian.

Although the implications for planet formation remain somewhat ambiguous, in that they depend strongly on the disk viscosity, the results of this paper show that planets with large semimajor axes (those with $a \approx 100$ AU) should be rarely produced in heavily populated star clusters. After 1 Myr have elapsed, disks are either completely dispersed, or are truncated to radii $r_d < 100$ AU (see Figure 7).

Future research can be taken in several directions. The time-dependent disk model developed in this paper can be used to study a wider variety of systems, with parameters outside of the range explored herein. In particular, we have only considered systems with host stars $M_* = 1\,M_\odot$. Considering stars with larger masses is especially important, because massive stars produce deeper gravitational potential wells, which could allow their disks to resist being photoevaporated. As mentioned previously, one goal of this paper is to identify the relative importance of internally versus externally generated radiation fields. This paper has made progress in addressing this issue, but much work still remains. It is important to emphasize that the most important factor in this issue is the environment in which the disk resides—many disks living in relative isolation will never be exposed to the damaging photoevaporating fields discussed in this paper, and hence this discussion is restricted to objects in more populated clusters. We have shown that for disks around solar-mass stars, the effects of X-ray illumination from the host star are usually insignificant compared to the effects of external FUV illumination. However, we have not considered FUV radiation from the host star itself. Gorti et al. (2009) find that for a viscosity of $\alpha = 10^{-2}$, disks are dispersed within ∼4 Myr, and for $\alpha = 10^{-3}$ disk lifetimes can exceed 10 Myr. For comparison, our model predicts that disks with $\alpha = 10^{-2}$ are effectively dispersed in less than 0.5 Myr and disks with $\alpha = 10^{-3}$ within 1–3 Myr (see Figure 9). Comparing these time scales for disk dispersal, FUV fields from the host star are not expected to drastically alter the results of this paper, but they could provide corrections of, perhaps, factors of order unity, and should be included in future calculations.

This paper benefited from discussions with many colleagues, especially Jaehan Bae, Konstantin Batygin, and James Owen. We also thank an anonymous referee for useful comments. K.R.A. and N.C. were supported in part by NASA Origins Grant NNX08AH94G; F.C.A. was supported in part by NASA Origins grant NNX11AK87G.

REFERENCES

Adams, F. C. 2010, ARA&A, 48, 45
Adams, F. C., Hollenbach, D., Laughlin, G., & Gorti, U. 2004, ApJ, 611, 360
Alexander, R. D., Clarke, C. J., & Pringle, J. E. 2006, MNRAS, 369, 229
Armitage, P. J. 2000, A&A, 362, 968
Armitage, P. J. 2011, ARA&A, 49, 195
Bally, J., O'Dell, C. R., & McCaughrean, M. J. 2000, AJ, 119, 2925
Bergin, E., Calvet, N., D'Alessio, P., & Herczeg, G. J. 2003, ApJL, 591, L159
Brandenburg, A., Nordlund, A., Stein, R. F., & Torkelsson, U. 1996, ApJL, 458, L45
Clarke, C. J. 2007, MNRAS, 376, 1350
Clarke, C. J., Gendrin, A., & Sotomayor, M. 2001, MNRAS, 328, 485
D'Alessio, P., Calvet, N., Hartmann, L., Lizano, S., & Cantó, J. 1999, ApJ, 527, 893
Eisner, J. A., Plambeck, R. L., Carpenter, J. M., et al. 2008, ApJ, 683, 304
Ercolano, B., Clarke, C. J., & Drake, J. J. 2009, ApJ, 699, 1639
Fatuzzo, M., & Adams, F. C. 2008, ApJ, 675, 1361
Flaccomio, E., Micela, G., & Sciortino, S. 2012, A&A, 548, A85
Gammie, C. F. 2001, ApJ, 553, 174
Getman, K. V., Feigelson, E. D., Broos, P. S., Micela, G., & Garmire, G. P. 2008, ApJ, 688, 418

Gorti, U., Dullemond, C. P., & Hollenbach, D. 2009, ApJ, 705, 1237
Gorti, U., & Hollenbach, D. 2009, ApJ, 690, 1539
Güdel, M., Briggs, K. R., Arzner, K., et al. 2007, A&A, 468, 353
Habing, H. J. 1968, BAN, 19, 421
Henney, W. J., & O'Dell, C. R. 1999, AJ, 118, 2350
Hernández, J., Hartmann, L., Calvet, N., & Jeffries, R. D. 2008, ApJ, 686, 1195
Hillenbrand, L. A., & Hartmann, L. W. 1998, ApJ, 492, 540
Holden, L., Landis, E., Spitzig, J., & Adams, F. C. 2011, PASP, 123, 14
Hollenbach, D., Johnstone, D., Lizano, S., & Shu, F. 1994, ApJ, 428, 654
Johnstone, D., Hollenbach, D., & Bally, J. 1998, ApJ, 499, 758
Lada, C. J., & Lada, E. A. 2003, ARA&A, 41, 57
Lynden-Bell, D., & Pringle, J. E. 1974, MNRAS, 168, 603
Mann, R. K., & Williams, J. P. 2009, ApJL, 694, L36
Mann, R. K., & Williams, J. P. 2010, ApJ, 725, 430
Menten, K. M., Reid, M. J., Forbrich, J., & Brunthaler, A. 2007, A&A, 474, 515
Mitchell, T. R., & Stewart, G. R. 2010, ApJ, 722, 1115
O'Dell, C. R., Wen, Z., & Hu, X. 1993, ApJ, 410, 696
Owen, J. E., Clarke, C. J., & Ercolano, B. 2012, MNRAS, 422, 1880
Owen, J. E., Ercolano, B., & Clarke, C. J. 2011, MNRAS, 412, 13
Owen, J. E., Ercolano, B., Clarke, C. J., & Alexander, R. D. 2010, MNRAS, 401, 1415
Pollack, J. B., Hubickyj, O., Bodenheimer, P., et al. 1996, Icar, 124, 62
Preibisch, T., Kim, Y.-C., Favata, F., et al. 2005, ApJS, 160, 401
Pringle, J. E. 1981, ARA&A, 19, 137
Richling, S., & Yorke, H. W. 2000, ApJ, 539, 258
Shakura, N. I., & Sunyaev, R. A. 1973, A&A, 24, 377
Shu, F. H., Tremaine, S., Adams, F. C., & Ruden, S. P. 1990, ApJ, 358, 495
Störzer, H., & Hollenbach, D. 1999, ApJ, 515, 669
Vicente, S. M., & Alves, J. 2005, A&A, 441, 195
Wang, J., Townsley, L. K., Feigelson, E. D., et al. 2008, ApJ, 675, 464
Williams, J. P., & Cieza, L. A. 2011, ARA&A, 49, 67